AFRL-AFOSR-JP-TR-2021-0006

Demonstrating a Magic Interrogation Approach for a Two-Photon Atomic Clock

Luiten, Andre
THE UNIVERSITY OF ADELAIDE
NORTH TERRACE
ADELAIDE, SA, 5005
AUS

08/02/2021
Final Technical Report

Air Force Research Laboratory
Air Force Office of Scientific Research
Asian Office of Aerospace Research and Development
Unit 45002, APO AP 96338-5002

REPORT DOCUMENTATION PAGE

Form Approved
OMB No. 0704-0188

1. REPORT DATE *(DD-MM-YYYY)*	**2. REPORT TYPE**	**3. DATES COVERED** *(From - To)*
02-08-2021	Final	06 May 2019 - 05 May 2020

4. TITLE AND SUBTITLE
Demonstrating a Magic Interrogation Approach for a Two-Photon Atomic Clock

5a. CONTRACT NUMBER
FA2386-19-1-4054

5b. GRANT NUMBER

5c. PROGRAM ELEMENT NUMBER

6. AUTHOR(S)
Andre Luiten

5d. PROJECT NUMBER

5e. TASK NUMBER

5f. WORK UNIT NUMBER

7. PERFORMING ORGANIZATION NAME(S) AND ADDRESS(ES)
THE UNIVERSITY OF ADELAIDE
NORTH TERRACE
ADELAIDE, SA 5005
AUS

8. PERFORMING ORGANIZATION REPORT NUMBER

9. SPONSORING/MONITORING AGENCY NAME(S) AND ADDRESS(ES)
AOARD
UNIT 45002
APO AP 96338-5002

10. SPONSOR/MONITOR'S ACRONYM(S)
AFRL/AFOSR IOA

11. SPONSOR/MONITOR'S REPORT NUMBER(S)
AFRL-AFOSR-JP-TR-2021-0006

12. DISTRIBUTION/AVAILABILITY STATEMENT
A Distribution Unlimited: PB Public Release

13. SUPPLEMENTARY NOTES

14. ABSTRACT
See attached

15. SUBJECT TERMS

16. SECURITY CLASSIFICATION OF:			**17. LIMITATION OF ABSTRACT**	**18. NUMBER OF PAGES**	**19a. NAME OF RESPONSIBLE PERSON**
a. REPORT	**b. ABSTRACT**	**c. THIS PAGE**			CHRISTOPHER VERGIEN
U	U	U	SAR	15	**19b. TELEPHONE NUMBER** *(Include area code)* 315-227-7002

Final Report: Demonstrating a Magic Interrogation Approach for a Two-Photon Atomic Clock

Basic Research for AOARD Proposal 19IOA054 "Demonstrating a Magic Interrogation Approach for a Two-Photon Atomic Clock", dated 30 JUL 2018

Prepared by: Sarah Scholten, Chris Perrella, Jacinda Ginges, Andre Luiten.
Affiliation: University of Adelaide.
UoA Reference: 0006006219
Award Number: FA2386-19-1-4054
WS00180868
Date: 3rd August 2020

Background

Both the University of Adelaide and AFRL have been constructing vapour-cell atomic optical frequency standards which aim to provide frequency stability performance matching or exceeding that of the highest-stability commercial frequency standards (e.g. a *Microsemi* MHM-2010 H-Maser), but do it with a ~10-fold reduction in SWaP.

The fundamental approach is based around frequency locking a laser source to a two-photon $5S_{1/2} \rightarrow 5D_{5/2}$ transition in a heated Rb vapour cell. The AFRL clock takes the approach of a single colour excitation of this transition using two 778nm photons, while the Adelaide group uses two *different* wavelength photons at 780nm and 776nm for the excitation (see Figure 1). In both cases, the excitation is performed using counter-propagating fields to provide a high level of suppression of Doppler broadening. In the AFRL case, this yields a transition bandwidth of around ~300kHz, while the Adelaide group obtains a degraded linewidth of 4MHz because of the use of the two colours. However, on the other hand, the more complex dual-colour scheme has an advantage in that it produces a 1000-fold increase in the strength of the two-photon interaction. The principal technical benefit of this increased interaction strength is to create a similar signal-to-noise ratio with a 1000-fold reduction in excitation power. Both frequency standards detect 420nm fluorescence (see Figure 1) to ensure that the two-photon excitation is frequency locked to the atomic transition.

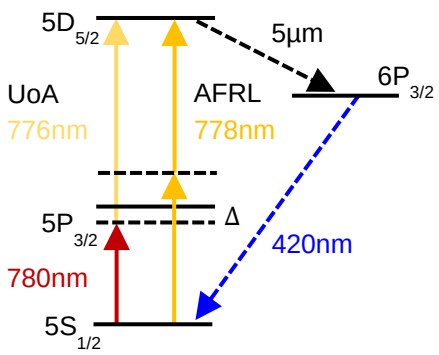

Figure 1: Two-colour two-photon Rubidium excitation scheme. UoA excitation scheme (left) and AFRL excitation scheme (right)

Motivation for the Research

At first sight, one might have believed that the lower powers used in Adelaide's two-colour scheme might have delivered an advantage over the AFRL single colour excitation by providing a smaller light shift [1-5]. However, a simple argument shows that this is not true. Ignoring complexities associated with polarisation and optical pumping, the unwanted optical light shift, Δf, depends on the laser

frequency detuning from the intermediate $5P_{3/2}$ energy level, Δ, along with the laser intensities of the two counter-propagating fields, I_1 and I_2, in the form:

$$\Delta f \propto \frac{\mu_1^2 I_1}{\Delta} - \frac{\mu_2^2 I_2}{\Delta} \quad (1)$$

Where $\mu_{1,2}$ is the transition matrix element is of the 1st and 2nd transition of the two-photon transition. The excitation rate of the two-photon transition (which essentially sets the intrinsic performance of the clock) is proportional to the product of the driving laser intensities:

$$W \propto \frac{\mu_1^2 \mu_2^2 I_1 I_2}{\Delta^2} \quad (2)$$

The transition rate, W, is directly related to the fluorescence from the atomic vapour. We detect 420nm fluorescence, see Figure 1, as a measure of successful excitation of the two-photon transition. We process this fluorescence signal to steer the lasers' frequencies to ensure they are tuned to the two-photon transition. The noise of the fluorescence signal, which limits the clock stability, is determined by the shot-noise, $\sqrt{W}$. Thus, the Signal-to-Noise Ratio is given by:

$$SNR \propto \frac{W}{\sqrt{W}} = \sqrt{W} \quad (3)$$

If we compare the two approaches with the same transition rate (such that the intrinsic frequency stability limits of the two clocks are about the same), and with the intensities of the two-colour beams approximately the same, $I_1 \sim I_2 \sim I$, then we see an optical light shift that is independent of the frequency detuning and depends only on the requested transition rate:

$$\Delta f \propto \frac{\mu_1^2 - \mu_2^2}{\sqrt{\mu_1^2 \mu_2^2}} \sqrt{W} \quad (4)$$

Equation 4 tells us that both the two colour and single colour approach will yield approximately the same sensitivity to incident power fluctuations in circumstances where the dual colour excitation beams have about the same power.

Significance and Innovation

However, this analysis now points to a potential advantage of the dual colour scheme – if we adjust the power of each laser separately, we can alter the magnitude of the light shift while maintaining a given transition rate. In particular, by adjusting I_1/I_2 to be equal to μ_2^2/μ_1^2, we obtain a zero-light shift in Eqn. 1, while with $I_1 I_2 = I^2$ we maintain the original transition rate. This approach can deliver a substantial advantage – that any power fluctuations of the two lasers do not translate into changes in the optical frequency. This offers the potential for a substantial reduction in the frequency instabilities in the output of the clock over the medium (hours) and long (days) observation periods.

A similar possibility exists for the single colour excitation AFRL clock. In this case, one can add an additional light field to co-propagate with the existing single colour excitation. This additional field would be detuned from the transition such that it will not add any additional atomic excitation but, through its own light shift, will have the effect of shifting the clock state transition by an amount with exactly the same magnitude as the clock probe light, but with the opposite sign. Thus, as with the two-colour clock, we will realize a substantially reduced frequency shift for any laser power fluctuations. Of course, this would come with the disadvantage of the increased complexity.

Phase 1 (Year 1): Characterisation of Light Shifts

In the first year of this project (Phase 1) three tasks will be carried out. These are:

Task 1: Improve Stabilization of Optical Power (4 Months duration)

To accurately measure the light shifts induced by the probing lasers, the stability of both lasers driving the two-photon transition needs to be improved. This will also greatly improve the stability of the clock and its long-term performance.

Task 2: Measure & Model Light Shifts (5 Months duration)

Following Task 1 the optical powers driving the atomic transition will be stabilized and accurate, and precise measurements of the light shifts can be made. The light shifts will be measured as the excitation laser powers, polarization, and wavelengths are changed. In parallel we will develop the theoretical tools to explore the effect of the light shifts on two-photon transitions for both clocks at Adelaide and AFRL. We will take into account the effect of laser power, polarization (essentially a vector light shift), and wavelength.

Task 3: Improve Stabilization of Control Loops (3 Months duration)

To further minimize technical effects that masquerade as light shifts, the clock's control systems will be improved. The control loops that stabilize the frequency of both lasers and temperatures of critical components will be improved to minimize technical problems that masquerade as light shifts. The control loops that stabilize both laser frequencies will be improved to remove technical noise and increase flexibility in order to characterize light shifts over a large range of intermediate state detunings.

Tasks 1 & 3 will be solely carried out at UoA, along with the experimental component of Task 2. Theoretical modelling of the Light Shifts in Task 2 will be carried out in collaboration with UQ. Funding became available for this project at the beginning of July 2019. Progress towards each of these tasks is discussed below.

Task 1: Improve Stabilization of Optical Power

To produce accurate measurements of the effect of light shifts upon the clock, the optical powers of the lasers, that drive these shifts, need to be stabilised.

We have made modifications to the clock's setup that have improved power stability, which have in turn also led to an improvement in the overall clock stability. This work has included:

- Minimising optical interference at the power monitor photodiodes that create fictitious changes in optical power and designs for a new optical setup that avoids these issues.
- Investigating the separation of both 780nm and 776nm lasers for power control from a single beam using a dichroic filter and designs for a protocol that achieves this in the temporal domain rather than spatial domain.
- Implementation of a Residual Amplitude Modulation (RAM) cancellation scheme which minimises systematic offsets and drift in the two-photon control loop.

Each of these bodies of work are discussed in detail below. The culmination of this work will be the implementation of a new power control scheme in the near future. Note that several of these improvements also fall under Task 3: Improve Stabilisation of Control Loops.

Optical Interference at Power Monitors

In the current clock design, the optical powers of the two lasers are measured after passing through the rubidium (Rb) cell and physics package, see Figure 2, in which the two-photon transition is excited and the 420nm fluorescence measured for laser frequency control, as seen in Figure 1.

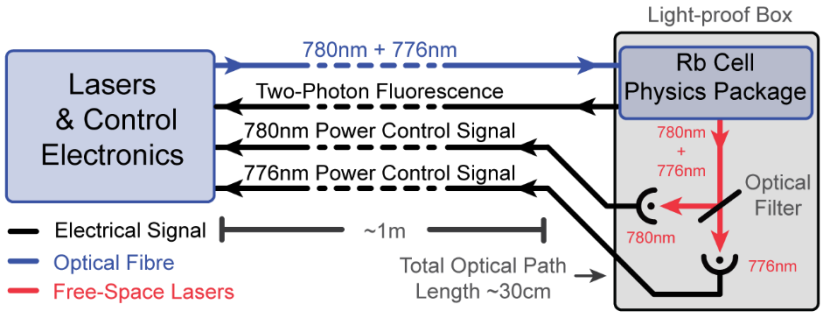

Figure 2: Schematic of the systems layout showing the current power control setup using an optical filter to separate the two lasers after passing through the Rb cell and physics package.

Measuring the optical powers after the physics package introduces subtle issues that limit the ultimate power stability that can be achieved. This is a result of optical aberrations or errant reflections from within the physics package that can appear on the output light and are detected by the two photodetectors that measure and stabilise the power of each laser. This is problematic as any movement (caused by mechanical or thermal means) of these errant beams can be translated into apparent power fluctuations, which the power stabilisation systems then correct for. These power fluctuations may arise from the beams interfering with one another when focused onto the photodetectors for detection, beam clipping of the errant beams, or reflections simply changing strength with thermal changes. Camera imaging of the light emerging from the physics package, as well as prior to each photodetector as shown in Figure 3, reveals the extent of the problem.

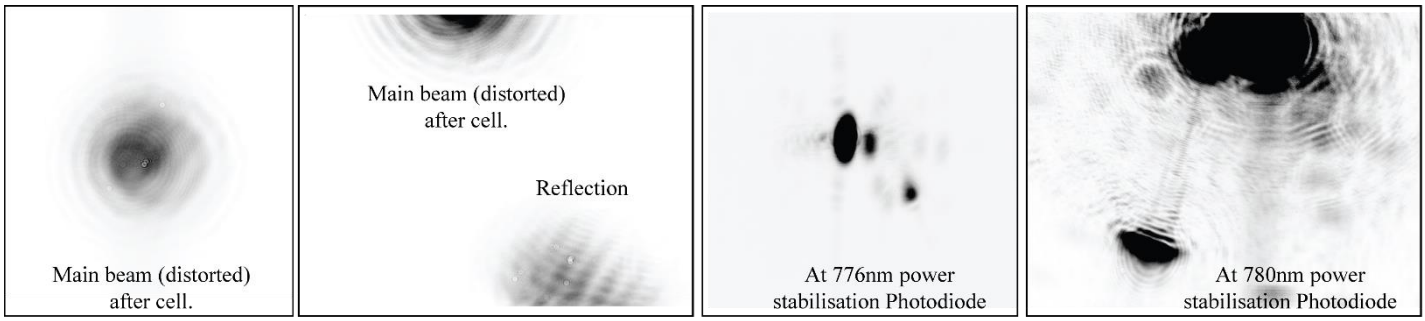

Figure 3: Camera images taken (from left to right) at the locations displayed in Figure 2: After the Rb Physics Package; before the 776nm power stabilisation photodetector; before the 780nm power stabilisation photodetector.

An iris placed prior to the optical filter that splits the two wavelengths for detection can effectively block the extra beams originating from within the physics package, improving laser power (see Figure 4) and hence clock stability. However, this does not remove the distortions of the main beam. Additionally, light measured after the Rb cell within the physics package has the atomic absorption imprinted on it at the level of 1%, effectively coupling the optical powers to the amount of absorption by the Rb within the two-photon cell. This is problematic as the amount of absorption by the atoms is coupled to the atomic environment, so any fluctuation in this environment – such as a temperature change to the cell – will produce a measured power change and will be erroneously corrected by the power stabilisation loops.

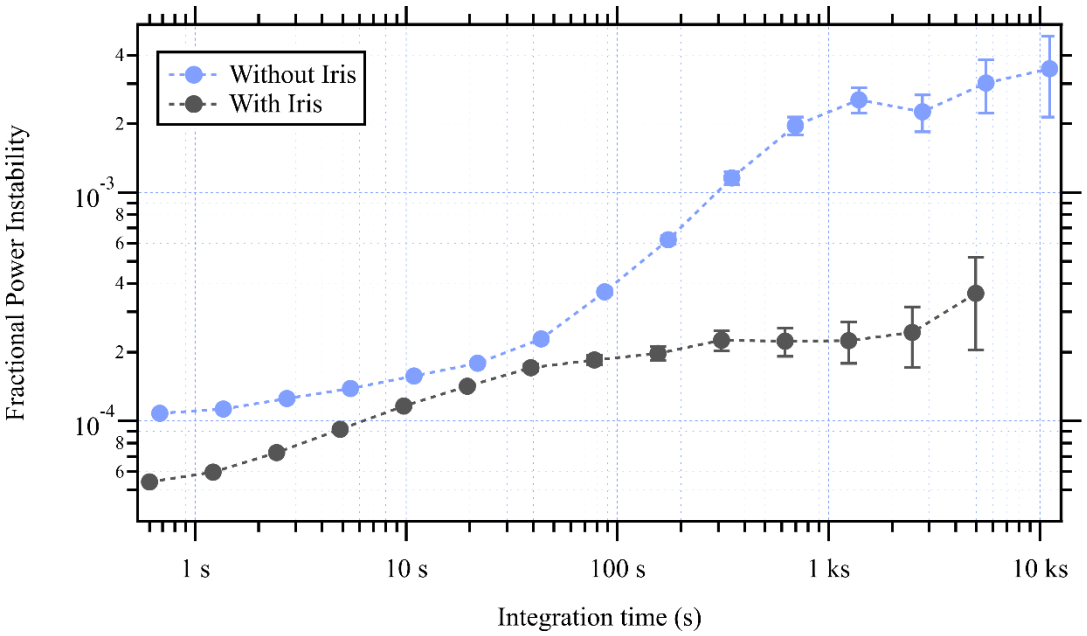

Figure 4: Power instabilities of the lasers with (grey) and without (blue) the iris in place after the physics package.

To counter both factors, we have redesigned the physics package to incorporate measurement of the optical powers prior to the Rb cell. An uncoated optical wedge will be used to reflect a small fraction of the input light prior to the Rb cell to a power stabilisation photodetector. The wedge is uncoated to prevent any polarisation dependent sensitivity which is commonly seen with coated or polarisation-based optics. The design of this setup is shown in Figure 5. Additionally, the second face of the optical wedge provides an opportunity for an additional laser power monitor separate from the stabilisation loop. This design has been 3D printed and is currently undergoing testing.

Separating both colours for power control

Currently a dichroic filter is being used to separate the spatially overlapped 780nm and 776nm lasers for power control. As these two lasers are so close in wavelength (4nm) it is difficult to build a dichroic filter with a large contrast between the two wavelengths. For the filter we are currently using, there is 5% cross-contamination between the 780nm and 776nm outputs as the filter cannot fully differentiate between the wavelengths. Furthermore, due to the steep wavelength cut-off of the filter, required to differentiate between 780nm and 776nm, the filter's contrast between the beams changes with temperature and polarisation leading to long term drifts in the power of the laser and thus light shifts.

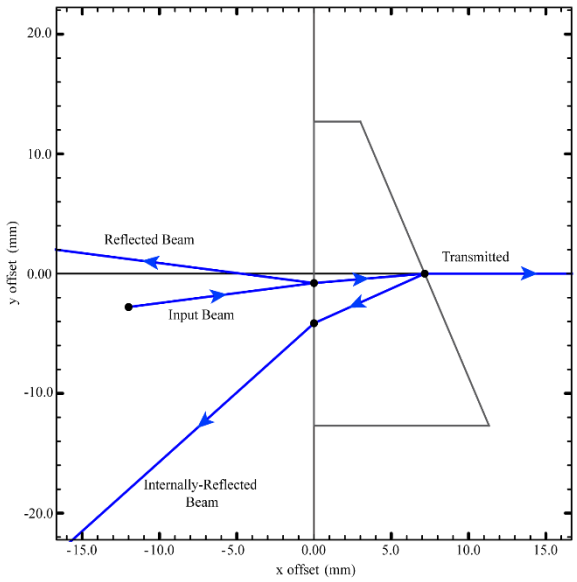

Figure 5: Schematic of the new wedge-based design for power stabilisation prior to the Rb cell. By using an angled input beam, two reflections are produced for use in the power stabilisation loop and as an external power monitor.

To greatly eliminate the current temperature and polarisation sensitivity and reduce cross-contamination of the two power controls, we will move to an AC power control system. This will do away with all the optics to spatially discriminate between the two beams, and instead discriminate between the two beams temporally. Both the

780nm and 776nm beams will be pulsed and the different pulse sequences will allow us to discriminate between the two beams. This technique has many advantages:

- Removal of dichroic filter reducing temperature and polarisation sensitivity of the clock,
- Miniaturisation of optics after the Rb cell for power control, leading to smaller design,
- AC power control allows rejection of photodiode offsets and background light, improving laser power stability.

This scheme will greatly improve the stability of the power control systems, leading to a higher stability clock, and more precise measurements of the light shifts associated with each laser beam. This design does not rely on an optical filter to separate the two laser beams, instead relying on temporal separation using a field-programmable gate array (FPGA). However, it has also been designed in such a way that the current optical-filter based approach is still able to be used while the temporal separation scheme is explored.

Residual Amplitude Modulation

The method in which the two-photon frequency is stabilised was found to be causing an effect known as Residual Amplitude Modulation (RAM). To facilitate power stabilisation of the two lasers, each laser is equipped with an acousto-optic modulator (AOM) which are driven at 80MHz where the AOMs are at the peak of their efficiency curves. To stabilise the two-photon frequency, the 776nm laser path AOM is additionally frequency modulated at a rate of ≈ 51kHz. The depth of this modulation is currently required to be relatively large (several MHz) which sweeps the AOM drive frequency either side of its peak efficiency at a rate of ≈ 51kHz, creating a laser amplitude modulation at the frequency modulation rate that is present on the output of AOM. This process creates what is known as RAM, a modulation in the optical power of the 776nm laser at the frequency modulation frequency, ≈ 51kHz in this case. The 776nm laser power stabilisation feedback loop does not have the bandwidth to correct for fast power changes, and so the RAM affects clock stability. Two methods have been tested (analogue and digital variants) to detect and reduce the RAM, before an approach based on a Red Pitaya FPGA was employed permanently. The effect of the FPGA-based RAM cancellation on the RAM may be seen in Figure 6 and the effect on clock stability may be seen in Figure 13.

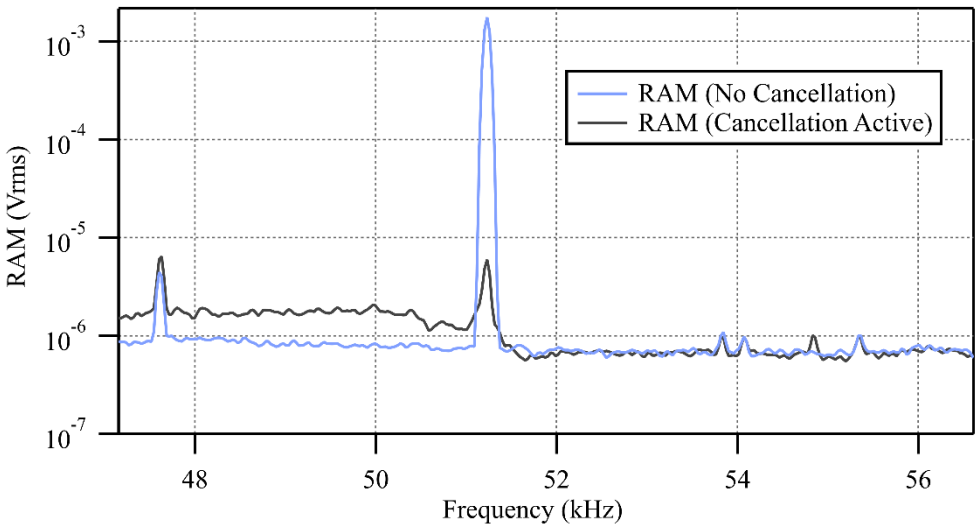

Figure 6: Spectrum of the measured residual amplitude modulation with (grey) and without (blue) active cancellation by the Red Pitaya FPGA.

Task 2: Measure & Model Light Shifts

Progress has been made for both measuring and modelling the light shifts of the ^{87}Rb $5S_{1/2} \rightarrow 5D_{5/2}$ two-photon transition. Two complementary models are being developed by Dr Jacinda Ginges (UQ) and Dr Chris Perrella (UoA). The model being developed at UQ analyses the effect of the light upon a single atom and builds this up from first principles by investigating the atomic wavefunction and it's polarizability. The model being developed at UoA studies the effect of the probing light upon an ensemble of thermal atoms in a vapour cell. By bringing these two complementary perspectives together, a deeper insight into the light shifts in this thermal Rb vapour will be gained, leading to more accurate theoretical calculations and thus tailoring the operation of the clock to a configuration that is more immune to light shifts. A brief discussion about the measurements and models are below.

Light Shift Measurements

The first measurements of light shifts have been made for the ^{87}Rb $5S_{1/2}(F = 2) \rightarrow 5D_{5/2}$ $(F = 4)$ clock transition utilised as the optical reference for our clock. Unfortunately, there are two mechanisms for power changes to translate into a frequency shift of the standard: the fundamental effect arising from light shifts from the atomic levels, and a wide range of technical effects within the control systems themselves (e.g. input offsets on control systems, gain sensitivities, thermal issues etc). We thus present these measurements as preliminary estimates as we need to verify that all of these unwanted technical sources of power sensitivity have been eliminated.

The process we have used to measure the light shifts is to modulate the power of each laser while measuring the output frequency of the clock. We find some unwanted cross-coupling between the measured power of the 780nm and 776nm due to our inability to effectively separate both colours using the current dichroic filter (as discussed in Task 1 above). The effect of this is that the expected and measured optical power for the two lasers does not represent the optical power that the atoms experience in the vapour cell. Implementation of the new optical power detection system and temporal discrimination, as discussed in Task 1 above, will significantly reduce those systematics. Nevertheless, Figure 7shows results for the light shifts due to changes in both the 780nm and 776nm optical powers. The expected dependence of the light shift, and thus clock output frequency, upon changing optical powers is a linear relationship as expressed in Eqn. (1). The observed light shift from

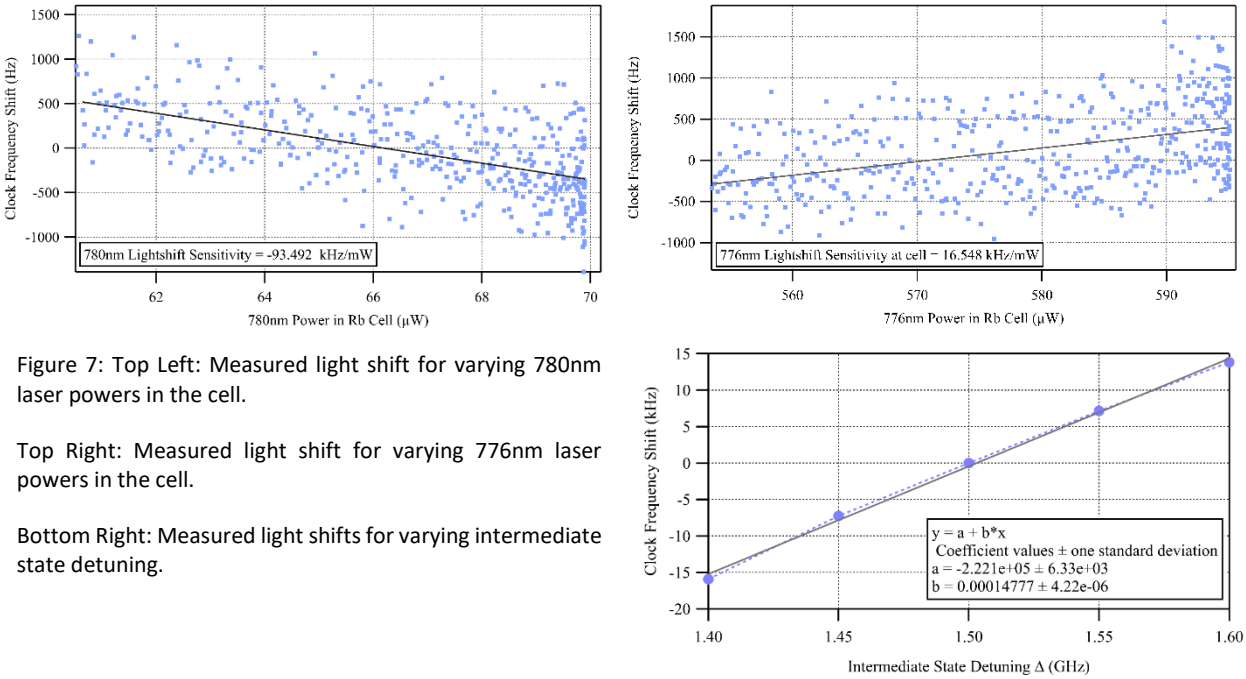

Figure 7: Top Left: Measured light shift for varying 780nm laser powers in the cell.

Top Right: Measured light shift for varying 776nm laser powers in the cell.

Bottom Right: Measured light shifts for varying intermediate state detuning.

changing the 780nm and 776nm laser power shows a linear dependence as expected for small perturbations in optical power, as shown Figure 7. The observed light shifts for 780nm and 776nm are 93.5kHz/mW and 16.5kHz/mW respectively. From a basic three level light shift model, the calculated light shifts are 419kHz/mW and 45.7kHz/mW for the 780nm and 776nm beams respectively which are within a factor of 4.5 and 3 of that measured. For larger changes in optical power, unexpected non-linear behaviours are observed which are currently under investigation. The observed ratio between the 780nm and 776nm light shift coefficients is approximately -6, whereas a theoretical factor of ≈ -10 is expected based on the transition matrix elements of the two transitions, again indicating that there are systematics affecting the current set of measurements.

Light Shift Models

Two complementary models are being developed to be able to predict the light shifts expected for varying effects of laser power, polarization, and wavelength. These models are based upon atomic physics calculations to model the atomic polarizability under these varying conditions, and an atomic density matrix model that models the absorption and emission processes involved in excitation of the two-photon transition under these same conditions. Both models are discussed below.

Atomic Polarizability

The atomic polarizability is found from relativistic atomic structure calculations. We use the high-precision correlation potential method to evaluate it, a method that works particularly well for the heavy alkali-metal atoms. This has been used to obtain some of the most accurate theoretical information for Rb, Cs, and Fr.

Table 1: Calculated reduced electric dipole matrix elements compared to experimental results.

$\lvert\langle k\rVert d\rVert 5s_{1/2}\rangle\rvert$ (a.u.)			$\lvert\langle k\rVert d\rVert 5p_{1/2}\rangle\rvert$ (a.u.)			$\lvert\langle k\rVert d\rVert 5p_{3/2}\rangle\rvert$ (a.u.)		
k	This	Expt.	k	This	Expt.	k	This	Expt.
$5p_{1/2}$	4.2442	4.2339(16)	$5s_{1/2}$	4.2442	4.2339(16)	$5s_{1/2}$	4.2442	4.2339(16)
$6p_{1/2}$	0.3205	0.3235(9)	$6s_{1/2}$	4.1344		$6s_{1/2}$	4.1344	
$5p_{3/2}$	5.9905	5.9760(23)	$4d_{3/2}$	8.0238	8.051(63)	$4d_{3/2}$	8.0238	8.051(63)
$6p_{3/2}$	0.5215	0.5230(8)	$5d_{3/2}$	1.3438		$5d_{3/2}$	1.3438	
						$4d_{5/2}$	8.0238	8.051(63)
						$5d_{5/2}$	1.3438	

The spectra of energy levels are discretised by placing the atom in a cavity. This improves the accuracy of the calculations by reducing the sum over (discrete and continuous) intermediate states in the polarizability to a sum over a pseudospectrum of discrete states, that match the physical states for the lowest-lying levels. To achieve this, we use a cavity of size 100 a.u.

Table 2: Scalar and tensor static polarizabilities in second-order and all-orders correlation potential with energy fitting.

Scalar α_0 and tensor α_2 static polarizabilities (a.u.)				
		$f\sum^{(2)}$	$f\sum^{(\infty)}$	Expt.
$5s_{1/2}$	α_0	319.1	319.9	319(6), 318.8(1.4)
$5p_{3/2}$	α_0	874.9	873.6	
	α_2	-166.2	-165.1	$-163(3)$
$5d_{5/2}$	α_0	16920	16910	
	α_2	-852.1	-839.8	

The form of the total polarizability depends on the laser polarization and the direction of the magnetic field that determines the quantization axis. It is ultimately built up from scalar, vector (for circular/elliptical polarization), and tensor components. We have performed calculations of the scalar and tensor polarizabilities for the dynamic (Figure 8) and static cases (Table 2), as well as the relevant E1 matrix elements (Table 1) and energy intervals that they are composed of, and compared against available experimental and theoretical data. Along with checks of the stability of the results, and estimates for the size of missed correlations and other effects, these provide an excellent gauge of the accuracy of the calculations. Our results demonstrate an accuracy on the level of 0.1% for the E1

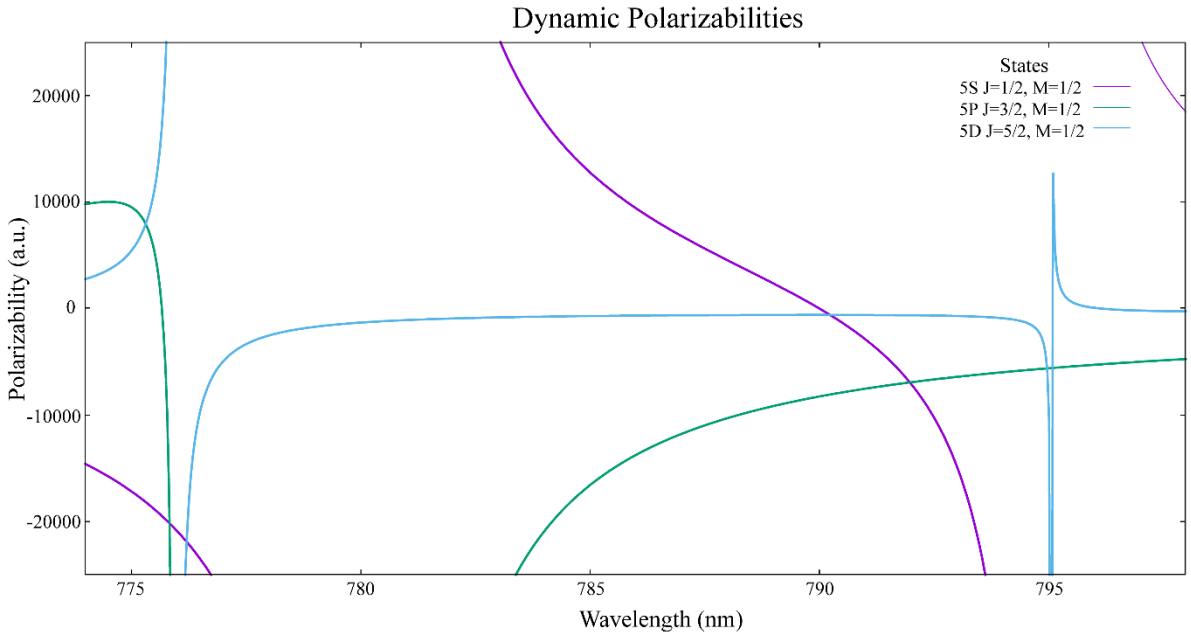

Figure 8: Frequency-dependent polarizabilities of Rb atoms in the ground, $5P$ and $5D$ states for linearly polarised light. Resonances can be observed at known transition frequencies: 776nm, 780nm, and 795nm.

matrix elements and transition energies.

Density Matrix Model

The density matrix model uses the Schrodinger equation to predict the time evolution, or steady state solution, to a light-atom interaction process. The physics of the interaction is captured in the combination of the Hamiltonian of an unperturbed atom (the atomic energy level structure), the interaction Hamiltonian of the light-atom interaction, and decay processes arising from natural decay or re-thermalisation of the atomic ensemble.

A density matrix model has been built up from a simple three energy level system to a system that resembles the hyperfine and Zeeman structure of the ^{87}Rb $5S_{1/2}(F = 2) \rightarrow 5D_{5/2}\ (F = 4)$ transition, shown in Figure 9. The output of this model is the fluorescence spectrum of the transition, shown in Figure 9, that is observable in the laboratory. This model includes population pumping effects, in which multiple interactions between the atom and light will change the population distribution of the atom significantly from a thermal vapour. This in turn changes the fluorescence spectrum of the transition leading to changes to the frequency at which the clock is stabilised. An important process in this population redistribution is re-thermalisation of the vapour within the laser beam due to atoms leaving the beam and atoms at thermal equilibrium entering the beam. This has roughly been included in the model and requires further validation.

Preliminary results from this model seen in Figure 9 which shows that the model is predicting the expected behaviour - light shifts that depend upon the optical intensity of each beam and shifts in

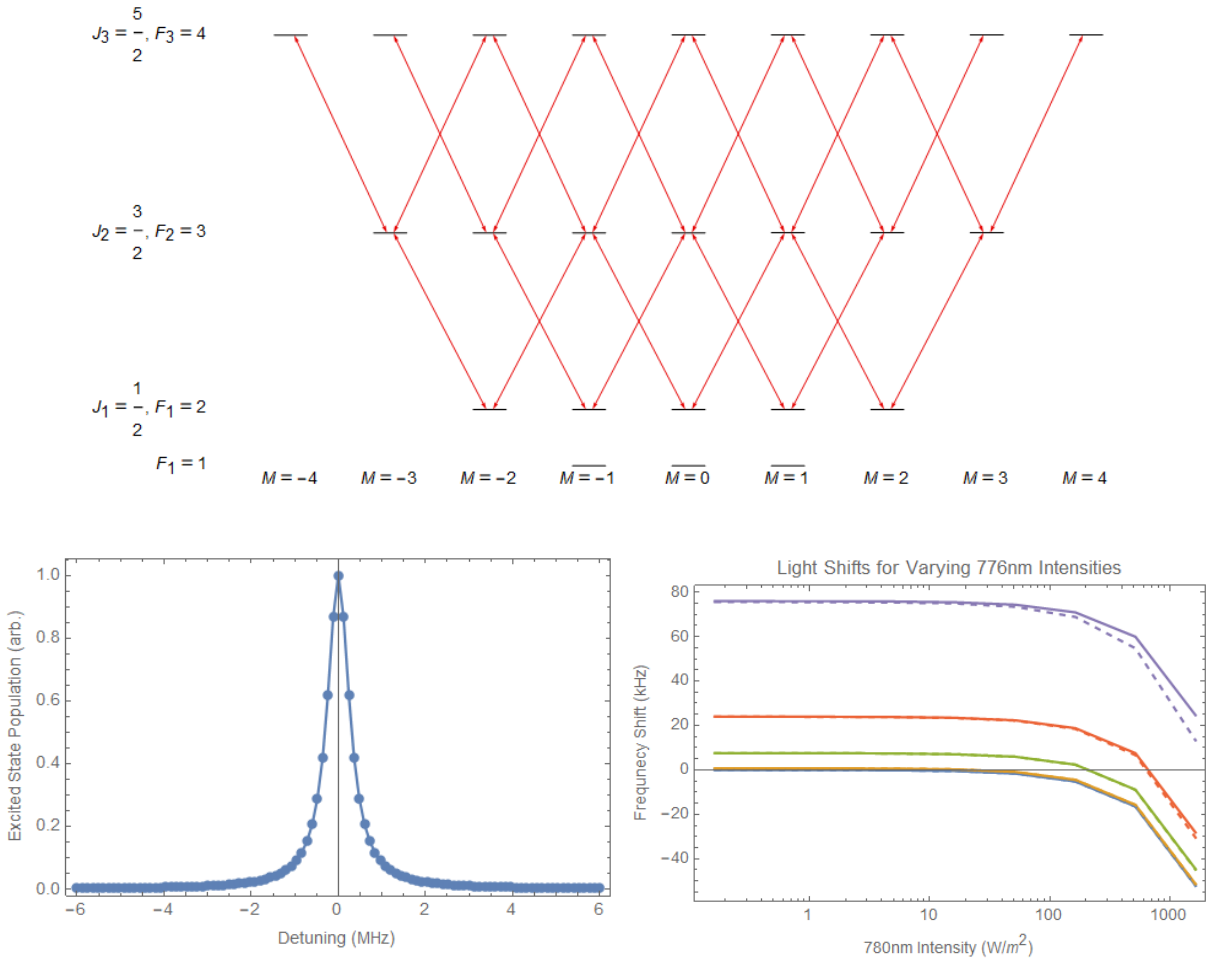

Figure 9: Top: Energy level diagram of the ^{87}Rb $5S_{1/2}(F = 2) \rightarrow 5D_{5/2}\ (F = 4)$ transition showing the ground, intermediate $5P_{3/2}(F = 3)$, and excited states that are involved in the excitation. Bottom Left: Population in the excited state that is a proxy for the 420nm fluorescence. Bottom Right: Light shifts extracted from the spectrum for zero light shift (solid lines) and 10% of Earth's field (dashed lines). Lines from bottom to top are 776nm intensities 3W/m^2, 300W/m^2, 3kW/m^2, 9kW/m^2 and 30kW/m^2.

opposite directions for the 780nm and 776nm laser powers. Excitingly, for each 776nm laser power, there is an 780nm optical power which completely cancels the light shift generated by the 776nm beam. It is this point at which we want to identify experimentally and where we want to operate the clock. A result of interest is that applying a small magnetic field (10% Earth's magnetic field) produces changes to the observed light shift for high optical powers where there is significant population pumping. More investigation into this will be required to fully understand this process.

Task 3: Improve Stabilization of Control Loops

Improvements to the control loops that stabilise the clock and measure the light shifts have been ongoing since the previous report and have made excellent progress. In addition to the RAM cancellation discussed in response to progress against Task 1: Improve Stabilisation of Optical Power, significant advancement has been made in the stability of the single-photon (780nm) transition.

Single Photon Detuning Stabilisation

To ensure high-precision measurements of the light shifts, a substantial amount of work has been put into the measurement systems to ensure high quality measurement are made. Since the last progress report, a completely self-contained and miniaturised single-photon (780nm) frequency stabilisation system has been designed, fabricated, tested, and integrated within the clock. The single-photon frequency lock is based on Saturable Absorption Spectroscopy (SAS), which allows a Doppler-free signal of the $5S_{1/2}$ $(F = 2) \rightarrow 5P_{3/2}$ $(F = 2,3)$ transition of ^{87}Rb to be measured and used to stabilise the 780nm laser frequency. The previous SAS system was quite large and relied on long BNC cables and bulky commercial photodetectors. Additionally, is was not particularly mechanically stable or isolated from ambient light sources.

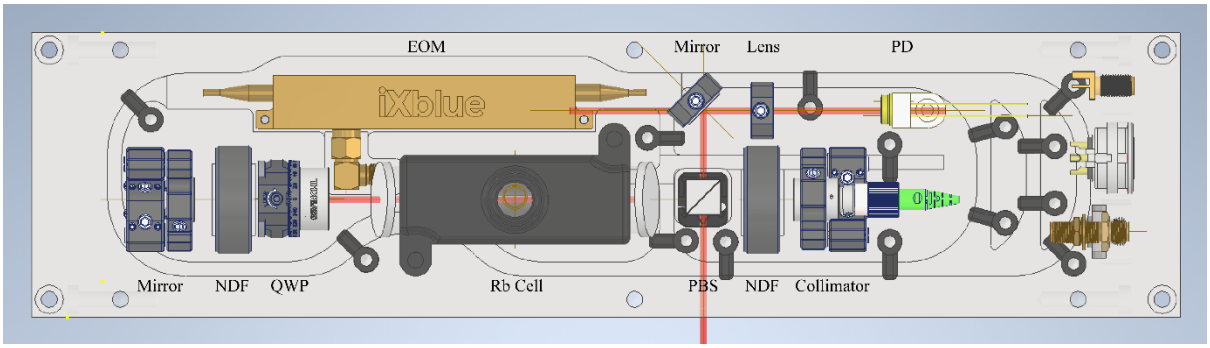

Figure 11: Top down view of the final design of the miniaturised SAS system, showing all components in place. NDF: neutral density filter; QWP: quarter waveplate; PD: photodiode; PBS: polarising beam splitter; EOM: electro-optic modulator. The fibre-coupled EOM is embedded within the baseplate.

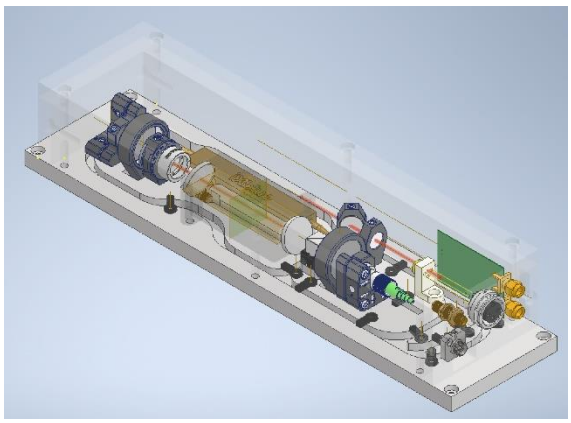

Figure 10: View of the final design with custom photodetector PCB and electrical pass through connections shown. The box that provides ambient light shielding is transparent in this image for clarity.

The new design is mechanically robust, with all components fixed to a rigid baseplate as seen in Figure 11. The optics are contained within a box that acts to shield the detectors within from ambient light sources. Electrical and optical pass-through connections are attached to one end of the box as seen on the right hand side in Figure 11 and in Figure 10. Additionally, photodetector electronics have been miniaturised onto a custom PCB that is also fitted within the box. These improvements to the SAS design translated into improved clock and single photon stabilities. The improvement to the single-photon stability is seen in Figure 12.

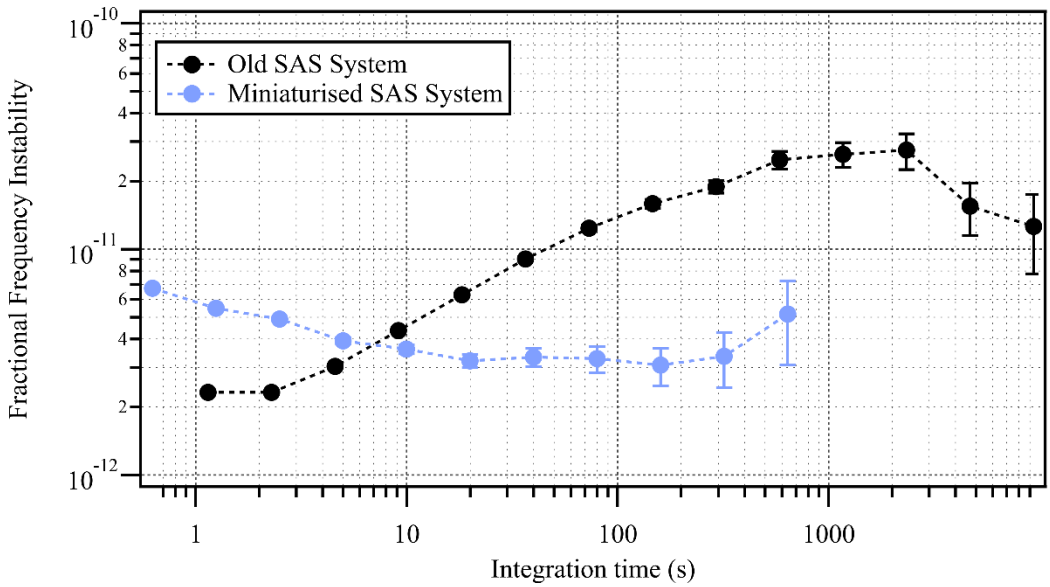

Figure 12: Frequency instabilities of the previous SAS system (black) compared to the miniaturised SAS (blue) as measured against the frequency comb. The miniaturised design shows excellent improvement at timescales of 10s and above compared to the previous version and is well away from interfering detrimentally with clock stability.

Current Frequency Stability Limitations

The previous progress report had identified that the clock was at that time limited by shot noise of the detected fluorescence at $t < 300$s. For longer times, $t > 300$s, the clock's frequency stability was limited by 780nm light shift. The stability presented in the progress report is shown in Figure 13.

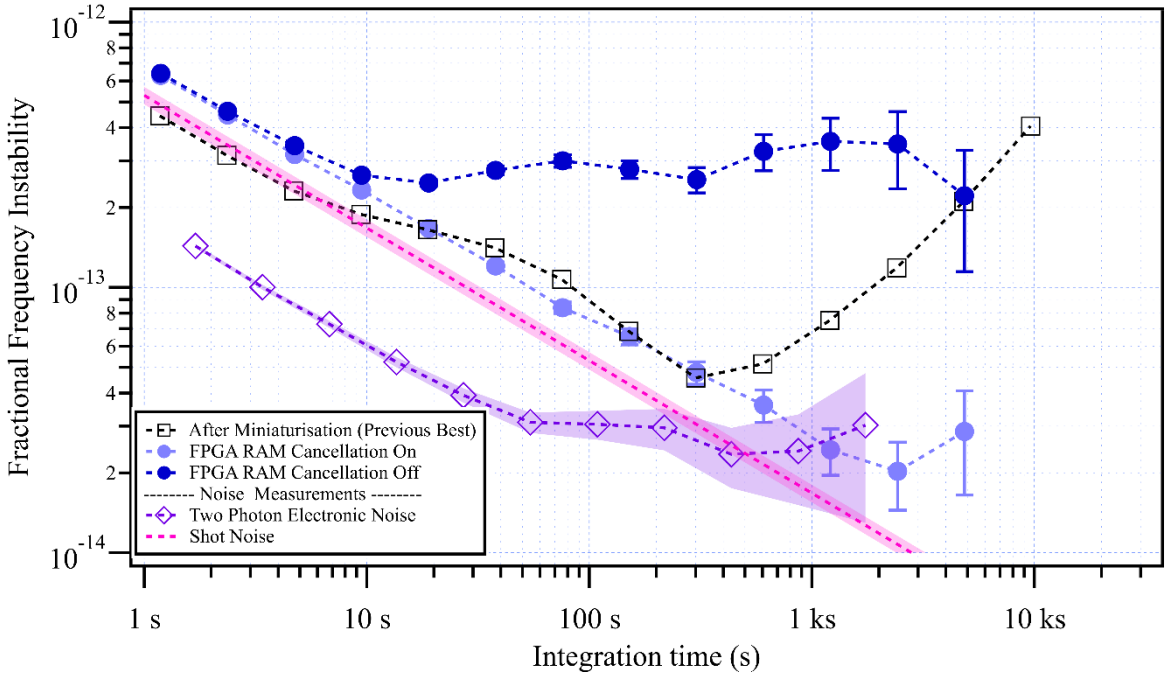

Figure 13: Frequency instabilities of the clock with (light blue) and without (dark blue) the RAM cancellation active. The previous best measurement with the fibre based Rb clock is shown in black for comparison. At shot time scales ($t < 10$s) shot noise (pink shading) is limiting the frequency stability. At long times ($t > 1000$s) the stability is limited by the electronic noise of the two-photon frequency lock (purple shading). Due to a purposeful reduction in 780nm power, light shifts generated by power fluctuations in either lasers are not currently a limitation (below scale of graph). Additionally, electronic noise of the two power locks also fall beneath the scales of the graph.

To mitigate the 780nm light shifts at long times-scales the power of the two 780nm and 776nm lasers have been adjusted to minimise the total light shift that clock experiences. When coupled with the improvements discussed in Tasks 1 and 3 above, this has resulted in an improved stability as presented in Figure 13. Current limitations to the clock's stability are shot noise at short timescales, $t < 1000$s, and electronic noise of the two-photon frequency stabilisation at longer timescales, $t > 1000$s. The former may be improved by increasing the amount of signal reaching the detector using the improved fluorescence capture described below in Phase 2. The latter will require a redesign of the electronics that stabilise the frequency of the two-photon transition. It has been noted that the two-photon stabilisation output is coupled to the surrounding temperature to a small but measurable extent. To correct for this, electronic components with improved thermal tolerancing will be used in the near future.

Phase 2 (Year 2): Characterisation of Light Shifts

A start has been made to the second year of the project. Specifically, Task 1 of Year 2: Improve Fluorescence Collection from the atoms, which will significantly increase the signal-to-noise ratio and minimize technical effects that masquerade as light shifts. This will allow higher precision tests of the light shifts and will also greatly improve the stability of the clock.

The current collection efficiency of the 420nm fluorescence is 0.13% determined by measuring the absorption of the 780nm and 776nm beams and comparing this to the power collected by the photomultiplier tube that measures the 420nm fluorescence. A proposed optical system for collecting significantly larger quantities of fluorescence is shown in Figure 14. A combination of mirrors and cylindrical lenses will surround the cell and focus the fluorescence onto two detectors either side of the Rb cell. The ray tracing for light fluoresced in the transverse plane to the laser propagation (shown in Figure 14) predicts 100% capture efficiency for a point source at the centre of the cell. To verify this optical geometry a commercial package (Zemax) will be used to verify the optical setup and extend the model into 3-dimensions to gain a better estimate of the collection efficiency. Expected collection efficiencies will still be above 20%, a 200-fold increase in fluorescence capture leading to more than

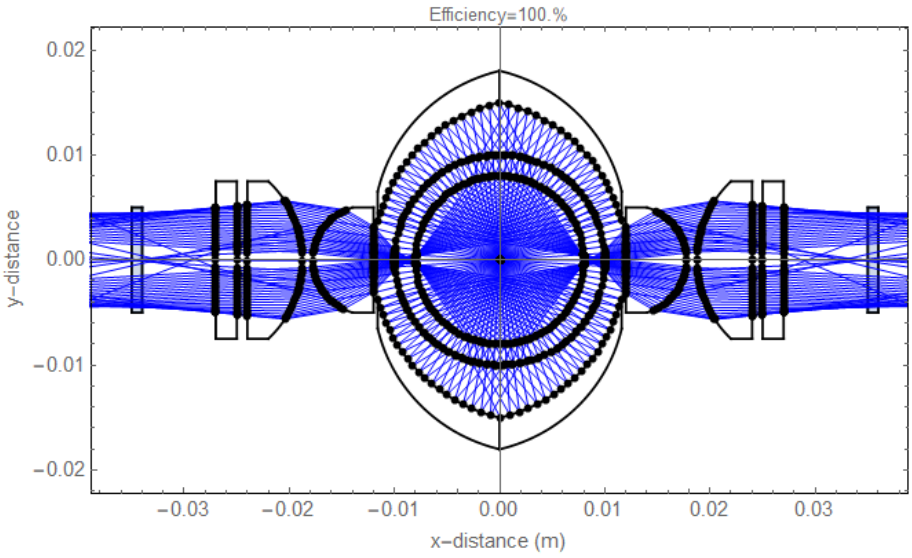

Figure 14: Cross section through the cell and collection optics. Ray tracing for a point source in the centre of the Rb cell (circles that represent the Rb cell cross section). The proposed fluorescence collection optics consist of mirrors above and below the cell that direct the light towards a fast (short focal length) and slow (slow focal length) lens to focus light onto two detector either side of the Rb cell at ± 35mm.

10-fold increase in clock stability and light-shift measurement precision. Prototyping of this optical geometry is currently being undertaken using 3D printed optical holders.

Future Work

Moving forwards there are three major experimental activities that are currently being tested, or will be undertaken in the near future:

- Increasing fluorescence capture – This will greatly increase our measurement precision by significantly increase the signal-to-noise ratio and minimize technical effects that masquerade as light shifts. This work falls under Task 1 of Year 2.
- Higher contrast wavelength separation – This will allow much better control of the optical powers that interact with the Rb vapour. As discussed above, we will move to an AC power control system to greatly eliminate the current temperature and polarisation sensitivity and reduce cross-contamination of the two power controls. This work falls under Task 1 and 3.
- Power monitoring without interferences – This will allow much higher power stabilities to be obtained increasing the accuracy of light shift measurements. As discussed above, we are implementing a new optical setup that utilises an uncoated wedge to monitor the beam powers. This work falls under Task 1 and 3.

For the theoretical work, there are two main areas of work that are soon to be undertaken, being:

- Atomic polarisation model will convert dynamic polarizabilities into hyperfine components – This will enable light shifts to be calculated for various experimental conditions. From here, this theory and experimental results can be compared leading to refinement of both aspects. This work falls under Task 2.
- Density matrix model will thoroughly integrate atomic re-thermalisation – This will make the model more closely resemble the reality of the experiment leading to more accurate light shift predictions. This model will be compared to the atomic polarisation model and experimental results. This work falls under Task 2.

Project Outputs

Based on the above progress and that planned over the next few months, we are expecting to be able to publish 3 papers from this project over the next year. These papers will report upon:

1. The stability of the clock with 1 second fractional frequency stabilities near or below 10^{-13} and stabilities at longer time scales reaching the 10^{-15} range.
2. Precise light-shift measurements and characterisation for the two-photon transition. Comparison to modelling and cancellation of the light shift using optical power balancing or polarisation control.
3. Accurate measurement of atomic parameters using the precision of the clock's frequency stability and refinement of Dr Jacinda Ginges atomic models.

References

[1] M. S. Safronova, C. J. Williams, and C. W. Clark, “Relativistic many-body calculations of electric-dipole matrix elements, lifetimes, and polarizabilities in rubidium,” *Phys. Rev. A - At. Mol. Opt. Phys.*, vol. 69, no. 2, p. 8, 2004.

[2] M. S. Safronova and U. I. Safronova, “Critically evaluated theoretical energies, lifetimes, hyperfine constants, and multipole polarizabilities in Rb87,” *Phys. Rev. A*, vol. 83, no. 5, p. 052508, May 2011.

[3] P. Siddons *et al.*, “Absolute absorption on rubidium D lines: comparison between theory and experiment,” *J. Phys. B At. Mol. Opt. Phys.*, vol. 41, no. 15, p. 155004, Aug. 2008.

[4] D. J. Whiting, J. Keaveney, C. S. Adams, and I. G. Hughes, “Direct measurement of excited-state dipole matrix elements using electromagnetically induced transparency in the hyperfine Paschen-Back regime,” *Phys. Rev. A*, vol. 93, no. 4, 2016.

[5] D. Sheng, A. Pérez Galván, and L. A. Orozco, “Lifetime measurements of the 5d states of rubidium,” *Phys. Rev. A*, vol. 78, no. 6, p. 062506, Dec. 2008.

[6] F. Nez, F. Biraben, R. Felder, and Y. Millerioux, “Optical frequency determination of the hyperfine components of the two-photon transitions in rubidium,” *Opt. Commun.*, vol. 102, no. 5–6, pp. 432–438, Oct. 1993.